Textures and Microstructures, 1988, Vols. 8 & 9, pp. 679–691
Reprints available directly from the publisher
Photocopying permitted by license only

Printed in the United Kingdom

Influence of Texture on $\mathbf{a}(\sin^2\psi)$ Curves Obtained from a Cold Rolled Nickel Sheet using Synchrotron Radiation

M. ECKHARDT and H. RUPPERSBERG

FB Ingenieurwissenschaften, Universität des Saarlandes, D-6600 Saarbrücken, FRG

(Received 29 July, 1987; in final form 20 November, 1987)

Dedicated to the memory of Professor Günter Wassermann

The Two-Axis Diffractometer at HASYLAB was used to measure $\mathbf{a}(\sin^2\psi)$ curves by reflecting synchrotron radiation from five different lattice planes of a cold rolled nickel sheet. We are especially interested in the complex surface state of the specimen and investigated the sample as delivered without further polishing and etching. Strongly non-linear $\mathbf{a}(\sin^2\psi)$ curves were observed. Most of them vary in a non-linear way if external uniaxial stress is applied. In this paper we study the influence of texture using formalism based on the ODF, and evaluated for the Reuss and the Voigt cases, respectively. Texture alone, however, is not sufficient to explain the whole variety of the observed effects.

KEY WORDS: Internal stresses, non-linear $\sin^2\psi$ curves, ODF-analysis, synchrotron radiation, nickel, cold rolled.

INTRODUCTION

We studied a commercial nickel plate, quality "R-Ni, No. 2.4066" manufactured according to DIN 17740. We are especially interested in the complex surface state which was formed after cold rolling the annealed specimen and studied the sheet as delivered without further polishing or etching. Ruppersberg *et al.* (1980) measured the lattice constant **a** by X-ray reflection from the (331) and (420) lattice

planes for different angles ψ and φ. ψ is the angle between the normal P_3 on the sheet and the direction L_3 in the laboratory system which intersects the direction between the primary and the diffracted beam. L_3 is perpendicular to the diffracting lattice planes. φ is the angle between the rolling direction and the intersection of the L_3–P_3 plane with the surface of the specimen.

The measurements were performed with and without external strain ε^a applied in the rolling direction. Instead of linear $\mathbf{a}(\sin^2\psi)$ curves, we observed a more or less pronounced non-linear behaviour with and without ψ-splitting, which means the observation of different $\mathbf{a}$ values for $-\psi$ and $+\psi$ (or ψ, φ; $\varphi + 180°$). Also the differential curves $\Delta\mathbf{a}(\sin^2\psi)$ calculated from $\mathbf{a}$ measured under two different applied strains were not linear. However straight lines were obtained if for a given ψ value $\mathbf{a}$ is plotted as a function of ε^a. Recently Eckhardt and Ruppersberg (1987) measured hardness, pole figures (PF) of intensity (I(ψ, φ), i.e. texture), PF of the lattice parameter ($\mathbf{a}(\psi, \varphi)$), PF of the line width ($\Delta\theta_{1/2}(\psi, \varphi)$) and they determined the variation of these quantities on annealing. With synchrotron radiation they studied $\mathbf{a}(\sin^2\psi, \varphi = 0, 180°)$ curves for the (220), (311), (222), (400) and (420) lattice planes with $\varepsilon^a = 0$, $\pm 0.4‰$ and $\pm 0.8‰$. Changing the wavelength λ through the absorption edge λ-K Ni of nickel, made it possible to study the (420) curves with the penetration depth varied by a factor of 6. In any case, most of the scattered intensity comes from a surface layer which is thinner than the mean grain diameter! None of the $\mathbf{a}(\sin^2\psi)$ curves is linear. There is a general tendency for negative $\mathbf{a}'' = d^2\mathbf{a}/(d\sin^2\psi)^2$ with in some cases superposed small ripples. $\langle\mathbf{a}'\rangle < 0$ for $\varepsilon^a = 0$. The mean slope $\langle\mathbf{a}'\rangle$ of the (420) curves becomes much more negative if the penetration depth is reduced by changing λ from above to below λ-K Ni. A superimposed tensile strain of $\varepsilon^a = 1‰$ would turn the latter curve approximately into the position observed with the larger penetration depth. We pointed out that comprehensive theoretical interpretation is premature and proposed the following conclusions as a working hypothesis: Compressive internal stress is responsible for $\langle\mathbf{a}'\rangle$ being negative. The strong differences between the (420) curves obtained with different penetration depth clearly indicate a rapid decrease of the compressive stress with increasing distance from the interface, and the resulting strain gradients are probably the reason for $\mathbf{a}'' < 0$.

Texture will add some modulations and the (*hkl*)-specific ripples are due to inhomogeneous plastic deformation. In this paper we will discuss the influence of texture.

FORMALISM

The use of X-ray stress analysis is a well established technique in the non destructive testing of polycrystalline materials. It consists in the determination of the lattice constant **a** as a function of ψ and—for more complete information—for several φ angles. An elastic deformation of isotropic homogeneous mediae yields the strain:

$$\varepsilon_{\varphi,\psi}(hkl) = \mathbf{a}/\mathbf{a}_o - 1 = \tfrac{1}{2}S_2(hkl)\sigma^{\mathrm{I}}_{\varphi}\sin^2\psi + S_1(hkl)(\sigma^{\mathrm{I}}_1 + \sigma^{\mathrm{I}}_2) \quad (1)$$

The σ^{I} values are macroscopic stresses parallel to the surface of the specimen. σ^{I}_1 and σ^{I}_2 are principal stresses. S_1 and S_2 are the X-ray elastic constants. φ in Eq. (1) is the angle between the intersection of the L_3–P_3 plane and the σ_1 direction which in general corresponds to the rolling direction. Deviations from Eq. (1) have often and long since been observed. Theoretical interpretation was given in terms of surface anisotropy, stress- or strain gradients, strain inhomogeneities related to second order stress σ^{II}, and texture.

Stickforth (1966) deduced a more complicated behaviour than given by Eq. (1) for the surface layer of the specimen. Theory, however, does not give quantitative information and experiments published by Hauk *et al.* (1985) show that this effect is of no practical importance though the X-ray often penetrate to a depth corresponding to little more or even less than the mean grain size.

A lot of work was done to take the influence of texture into account, starting from ideal texture components (e.g. Dölle and Hauk, 1978, I and II) and recently by making full use of orientation distribution functions (Brakman, 1983, Barral *et al.*, 1983). The starting points for the latter methods are the equations for the elastic behaviour of the single crystallites:

$$\varepsilon^{\mathrm{II}}_{ij} = s_{ijkl}\sigma^{\mathrm{II}}_{kl}; \qquad \sigma^{\mathrm{II}}_{ij} = c_{ijkl}\varepsilon^{\mathrm{II}}_{kl} \quad (2)$$

where $\varepsilon^{\mathrm{II}}$ etc. corresponds to $\varepsilon^{\mathrm{II}} + \varepsilon^{\mathrm{I}}$ in the Macherauch notation.

It is advantageous to use a "laboratory coordinate system" (L) to perform the averaging necessary for relating the macroscopic to the microscopic properties. The 3-axis of the L-system has the direction of the normal on the lattice plane investigated, i.e. $\varepsilon_{\varphi,\psi} \rightarrow \varepsilon_{33}^{L}$:

$$\varepsilon_{33}^{L} = \frac{1}{\mathbf{V}_d} \int_h \varepsilon_{33}^{\mathrm{II},L}\, d\mathbf{V}_d; \qquad \sigma_{ij}^{\mathrm{I},L} = \frac{1}{\mathbf{V}} \int_{\mathbf{V}} \sigma_{ij}^{\mathrm{II},L}\, d\mathbf{V} \tag{3}$$

The lefthand equation will be used to study the Reuss case (index R): $\sigma^{\mathrm{I}} = \sigma^{\mathrm{II}} \cdot \mathbf{V}_d$ corresponds to the total volume of the grains reflecting in the 3-direction. The integral has to be taken over all these grains. In the ODF the integration path follows a hairline $\mathbf{h}$. Such lines are given in Figure 1 for $\varphi = 0°$, different ψ-angles and for two lattice planes. $d\mathbf{V}_d$ corresponds to the differential volume of crystallites on one point of the hairline and is proportional to $g(\alpha, \beta, \gamma)$, the ODF at this special point: $d\mathbf{V}_d = g(\alpha, \beta, \gamma) \cdot d\alpha\, d\beta\, d\gamma$. α, β and γ are the Euler angles describing the orientation of the grains with respect to the specimen and we write for short: $\alpha, \beta, \gamma = \Lambda$. The second of the Eq. (3) is the basis for introducing the Voigt assumption (V): $\varepsilon^{\mathrm{I}} = \varepsilon^{\mathrm{II}}$, which means that $\varepsilon_{33}^{\mathrm{I},L} = \varepsilon_{33}^{L} = \varepsilon_{33}^{\mathrm{II},L}$. To obtain $\sigma_{ij}^{\mathrm{I},L}$ the integration has to be performed over the total volume $\mathbf{V}$. (2) and (3) yield for the R and V case, respectively:

$$\varepsilon_{33}^{L,R} = \left(\frac{1}{\mathbf{V}_d} \int_h s_{33kl}^{L}\, d\mathbf{V}_d\right) \sigma_{kl}^{\mathrm{I},L,R} \equiv R_{33kl}^{L,R} \cdot \sigma_{kl}^{\mathrm{I},L,R} \tag{4}$$

$$\varepsilon_{33}^{L,V} = \left[\frac{1}{\mathbf{V}} \int_{\mathbf{V}} c_{33kl}^{L}\, d\mathbf{V}\right]^{-1} \sigma_{kl}^{\mathrm{I},L,V} \equiv R_{33kl}^{L,V} \sigma_{kl}^{\mathrm{I},L,V}$$

$[\ ]^{-1}$ denotes the inverse tensor and

$$R_{33kl}^{L,R} = \frac{\int_h s_{33kl}^{L}\, g_{(\Lambda)}^{L}\, d\Lambda^{L}}{\int_h g(\Lambda)\, d\Lambda}; \qquad R_{33kl}^{L,V} = \left[\frac{\int_{\mathbf{V}} c_{33kl}^{L} g_{(\Lambda)}^{L}\, d\Lambda^{L}}{\int_{\mathbf{V}} g(\Lambda)\, d\Lambda}\right]^{-1} \tag{5}$$

In practice the integrations are performed with respect to the specimen coordinate system (more symmetry). The tensor is then inverted and transformed back to the laboratory system.

We finally have to turn back to the coordinates of the specimen (P) by means of the operator ($\rho_{ik}\,\rho_{jl}$) and obtain omitting the indices V or R:

$$\varepsilon_{\varphi,\psi} = (R^L_{33ij}\rho_{ik}\rho_{jl}) \cdot \sigma^{I,P}_{kl} = F_{ij}(\varphi, \psi, R^L_{33ij}) \cdot \sigma^{I,P}_{ij} \tag{6}$$

φ is the angle between the intersection of the L_3–P_3 plane and the 1-direction of the specimen, which for rolled sheets corresponds to the rolling direction. The 3-direction is perpendicular to the surface. The R^L_{33ij} depend on φ and ψ. If all $\sigma^{I,P}_{ij}$ excepted $\sigma^{I,P}_{11}$ vanish and for $\varphi = 0$, Eq. (6) reduces to

$$\begin{aligned}\varepsilon_{\varphi,\psi} &= F_{11}\sigma^{I,P}_{11} \\ &= [R^L_{3311} + (R^L_{3333} - R^L_{3311})\sin^2\psi + R^L_{3313}\sin 2\psi]\sigma^{I,P}_{11}\end{aligned} \tag{7}$$

For isotropic specimens one has: $R^L_{33ij} = S_1(hkl)\delta_{ij} + \frac{1}{2}S_2(hkl) \cdot \delta_{3i} \cdot \delta_{3j}$. Eq. (6) reduces to Eq. (1) with numerical values of S_1 and S_2 depending on whether R values calculated according to Reuss or Voigt are inserted. Linear $\varepsilon_{\varphi,\psi}(\sin^2\psi)$ curves are obtained in the Voigt case also for anisotropic specimen; S_1 and S_2 depending on the ODF (see Eq. (5)) or, more precisely, on the corresponding C^{11}_4, C^{12}_4 and C^{13}_4 expansion coefficients. In the Reuss case, linear $\varepsilon_{\varphi,\psi}(\sin^2\psi)$ curves are obtained in the case of textured samples only for the (hhh) and ($2h00$) reflections, at least if the specimen have orthorhombic or monoclinic symmetry. s^L_{33kl} in Eq. (5) remains unchanged along the (hhh)- and ($2h00$)-hairlines and (for the Reuss case!) the corresponding S_1 and S_2 values are not affected by texture. For general (hkl) they depend on all expansion coefficients of the ODF.

Finally it should be noted that the equations of mechanical equilibrium require (See Brakman, 1983) that at the surface of the specimen ($Z = 0$) $\sigma_{13}(Z) = \sigma_{23}(Z) = \sigma_{33}(Z) = 0$ and in addition $\partial\sigma_{13}(Z)/\partial Z = \partial\sigma_{23}(Z)/\partial Z = 0$ if both the stress and the strain tensors depend only on Z. In this case and in the absence of body forces we also have $\partial\sigma_{33}(Z)/\partial Z = 0$. Non zero σ_{13} and σ_{23} seem possible for more complicated nonhomogeneous specimens and for two (or more) phase materials. No ψ-splitting occurs for orthorhombic specimen symmetry. In all other cases ψ-splitting and/or curvature may be observed. Finit σ_{13} and σ_{23} will give rise to ψ-splitting and/or curvature in all cases.

EXPERIMENTAL

The Two-Axis Diffractometer which was used to perform the synchrotron radiation experiments at HASYLAB has been described elsewhere (Ruppersberg, 1981). The sample was irradiated with a monochromatic beam extending over about 7 mm in the horizontal and 4 mm in the vertical direction. The axis of the diffractometer was vertical. The wavelength was so chosen that the diffraction angles 2θ were about 160° with the exception of the (420) peak at $\lambda < \lambda$-KNi, for which 2θ came out to be 128°, and the (220) peak, for which $2\theta = 140°$ was chosen because the radiation which brings the peak to 160° is too strongly absorbed by air. Photographic registration of the diffracted beam showed uniformly blackened Debye–Scherrer rings. For registration of the diffracted beam a scintillation counter or a solid-state Ge detector was used with window sizes between $4 \times 4\ mm^2$ and $10 \times 10\ mm^2$. The counter windows were placed at distances between 40 and 100 cm from the diffractometer axis. For measuring $\mathbf{a}(\sin^2 \psi)$ the specimen was turned in ψ mode, i.e. about a horizontal axis. Peak positions were calculated from parabola fits through at least 12 points distributed at equal $\Delta(2\theta)$ about the peak maximum in the region of more than 80% maximum intensity. It took about 5 minutes to obtain one peak position with about 20,000 photons per point. In favorable cases a peak position could be reproduced within $\pm 0.003°$ (2θ) or even better. From time to time beam instabilities caused the peak to jump by two or three hundredths of a degree (2θ) and many results had to be rejected. Very problematical is the correct illumination of the sample. It is difficult to get the centre of gravity of the beam, which is always somewhat inhomogeneous, into the centre of the diffractometer, where the specimen is placed. It therefore take a long time to obtain sufficiently flat and horizontal $\mathbf{a}(\sin^2 \psi)$ curves for the powder samples used for calibration. Because of the restricted beam time we succeeded only by developing a computer program which simulates the resulting peak profiles and peak positions on taking all types of possible misalignments and the characteristics of diffractometers like extended source, Soller slits etc., into account. After chosing the 38 parameter describing the special diffractometer configuration it takes 20 minutes on a Siemens MX2 PC to simulate one $\mathbf{a}(\sin^2 \psi)$ curve.

External strain $-0.8‰ \leqq \varepsilon^a \leqq +0.8‰$ was applied by four point bending and controlled with a strain gauge attached to the backside of the nickel plate as well as by a dial gauge which allows precise determination of the amplitude of bending. The whole procedure including the question of homogeneity of strain distribution was checked in a separate experiment with 36 micro strain-gauges attached parallel and perpendicular to the 1-direction in the irradiated region of another nickel specimen cut from the same sheet. So we are sure that the ε^a values given correspond really to the elastic strain in 1-direction of the irradiated surface-region of the sample. We found no indication for constrained Poisson-contractions. $\mathbf{a}(\varepsilon^a)$ was found to be linear for all $-60° \leqq \psi \leqq +65°$ and all (hkl) investigated. Least square fits from the $\mathbf{a}(\varepsilon^a)$ *plots* yield $(d\varepsilon_{0,\psi}/d\varepsilon^a)$ which, devided by E, are plotted in Figures 3 and 4 as a function of $\sin^2\psi$. Individual $\mathbf{a}(\sin^2\psi)$ curves obtained at $\varepsilon^a = 0$ from the (400) plane and from the (420) reflection above and below λ-KNi are given in Figure 2.

The results presented for the (420) plane in the inset of Figure 2 have been obtained from a recent, very careful investigation, and we are sure that the hump shown really exists. The two curves which have been obtained from different adjacent sites on the specimen demonstrate that the shape of the hump varies somewhat on moving the sample, but it does not disappear. Photographic registration showed uniformly blackened Debye–Sherrer rings even on the top of the hump.

A general overview of the different $\mathbf{a}(\sin^2\psi)$ curves which we observed for the nickel specimen under investigation is given in the paper by Ruppersberg and Eckhardt (1987).

For the evaluation of texture, (111), (200) and (220) pole figures were determined using a back scattering texture diffractometer and Cu-K_α radiation. The pole figure showed some monoclinic distortion (Ruppersberg *et al.*, 1980) and were symmetrized before calculating the ODF. The ODF obtained using Bunge's program (1982) is shown in Figure 1.

RESULTS AND DISCUSSION

The maximum and minimum values of the ODF, Figure 1, are $g(\Lambda) = 0$ and 3.4, respectively, which shows that the texture is not

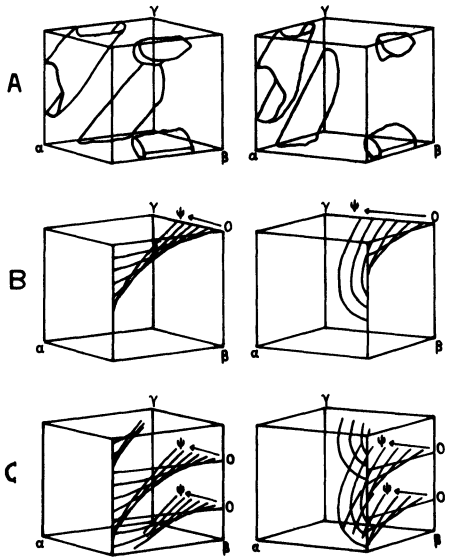

Figure 1 A: ODF $g(\Lambda)$ of the nickel specimen under investigation. Given are the contour faces for $g(\Lambda) = 2.2$. B: Hairlines of the integration path for calculating $R_{33kl}^{L_i R}$ according to Eq. (5) for the (400) reflection and $\varphi = 0°$. The lines are given for $\psi = 0°$ to $\psi = 60°$ in steps of 10°. C: Same as B for the (420) reflection. Right part of the figures: turned by 30° about the γ axis.

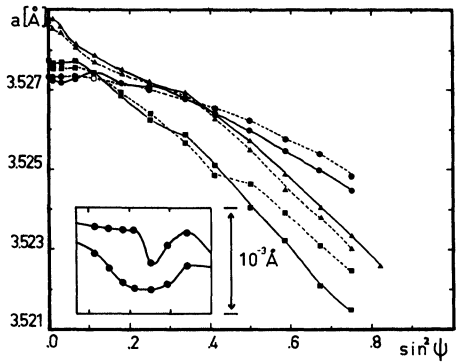

Figure 2 $\mathbf{a}(\sin^2\psi)$ curves for $\varepsilon^a = 0$. Full drawn curves: $\psi > 0°$, dashed curves: $\psi < 0°$; points: (420), $\lambda > \lambda$-KNi; squares: (420), $\lambda < \lambda$-KNi; triangles: (400). Insert: magnified curves for the (420) reflection, $\psi > 0°$, $\lambda > \lambda$-KNi; obtained at two different sites of the sample. The curves are shifted vertically with respect to each other.

strongly pronounced. The ODF given in Figure 1 shows the plane with $g(\Lambda) = 2.2$. The non-linear behaviour of the $\mathbf{a}(\sin^2\psi)$ curve observed for the (400) reflection with $\varepsilon^a = 0$, Figure 2, demonstrates that the internal state of the specimen is more complicated than described by the formalism outlined above. To check whether this formalism nevertheless correctly describes the relation between the macroscopic stress tensor and the strain $\varepsilon_{\varphi\psi}$ observed with X-rays, we investigated the variation of this strain, i.e. $\Delta\varepsilon_{\varphi\psi}$, on varying the stress in 1-direction by $\Delta\sigma_{11}^{I,P} = C_{1111}\Delta\varepsilon_{11}^{I,P} = E \cdot \varepsilon^a$. This allows to calculate from the experimental results the quantity $(d\varepsilon_{\varphi\psi}/d\sigma_{11}^{I,P}) = (d\varepsilon_{\varphi\psi}/E \cdot d\varepsilon^a)$, which according to Eq. (7) is equal to F_{11}. The E modulus $E = 204\ 10^3\,\mathrm{N\,mm^{-2}}$ was obtained experimentally for the given specimen. The F_{11} values obtained in this way are given in Figure 3 and 4 as circles and squares. They are compared with F_{11} values calculated according to Eq. (7) for the Reuss and the Voigt case, respectively, on the basis of the ODF and inserting for the single crystal coefficients the following values: $s_{11} = 7.95$, $s_{12} = -2.95$ and $s_{44} = -8.60^{-6}\,\mathrm{mm^2\,N^{-1}}$ (Bollenrath *et al.*, 1967). F_{11} calculated for the Reuss case of an isotropic specimen is given for some lattice planes as dashed lines.

The influence of texture is not very pronounced and strongest for the (311) and (420) reflections. The agreement between the F_{11} curves and the experimental values is satisfactory. For the (400) peak the experimental points lie on a perfectly straight line! Stronger deviations are observed only for the (420) peak including some ψ-splitting for $\lambda < \lambda$-KNi. The experimental values should be in the middle between the Reuss and the Voigt curves, but they are close to the Reuss results, at least in the case of (400) and (311) for which R and V are significantly different. (420) again looks more complicated. This behaviour may partly be due to erroneous single crystal coefficients which scatter quite strongly (see Bollenrath *et al.*, 1967); but it may as well be related to surface anisotropy, magnetostrictive effects, oxide layers, surface impurities etc., and at this stage it makes little sense to strive for a better fit by varying the single-crystal coefficients.

Another observation seems to be important for practical use: if the texture is not strongly pronounced then the $\mathbf{a}(\sin^2\psi)$ curves remain practically linear. Formal application of the $\sin^2\psi$-law, Eq. (1), however, will yield erroneous stress values or erroneous X-ray

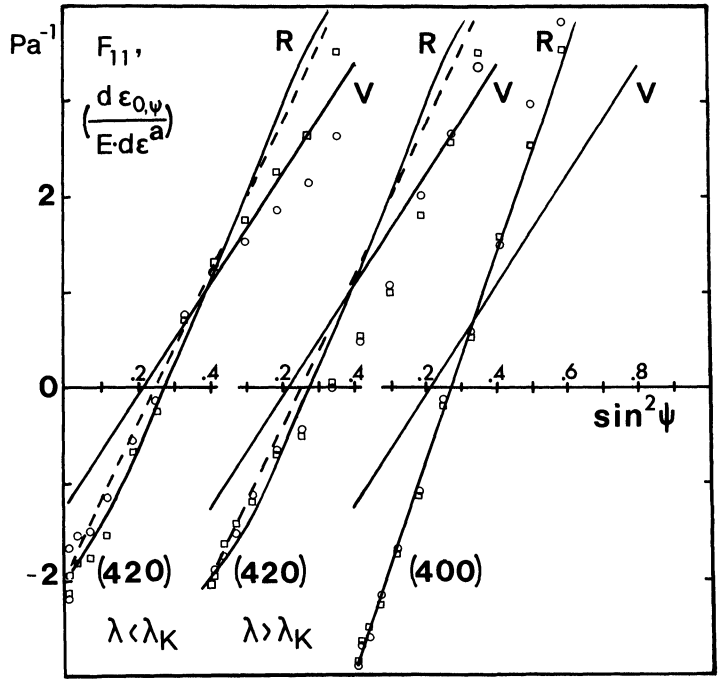

Figure 3 $(d\varepsilon_{0,\psi}/E \cdot d\varepsilon^a)$-values plotted versus $\sin^2\psi$ for the lattice planes given in the figure. □: $\psi > 0°$, ○: $\psi < 0°$. F_{11} $(\sin^2\psi)$ curves calculated according to Eq. (7) for the Reuss (R) and the Voigt (V) case, respectively. F_{11} $(\sin^2\psi)$ curves calculated according to Eq. (7) for isotropic nickel specimen using the Reuss assumption are given as dashed lines.

elastic coefficients. This latter fact may be explained regarding the almost linear curves $F_{11}^V(\sin^2\psi)$ and $F_{11}^R(\sin^2\psi)$ calculated taking texture into account for the (220) and (331) reflections and which are given in Figure 4. It was mentioned above that the curve $\frac{1}{2}(F_{11}^V + F_{11}^R)$ plotted against $\sin^2\psi$ will probably be close to $(d\varepsilon_{\varphi,\psi}/E\,d\varepsilon^a)$ obtained experimentally if there are only texture effects. Using Eq. (7) and formal application of Eq. (1) yields from $F_{11}^V(\sin^2\psi)$ and $F_{11}^R(\sin^2\psi)$ the $-S_1$ and $\frac{1}{2}S_2$ values given in the columns of Table 1 which are labelled "textured", and which deviate significantly from the corresponding values calculated for random specimen using the same elastic constants. The mean values calculated from the Voigt and the Reuss data of the textured sample

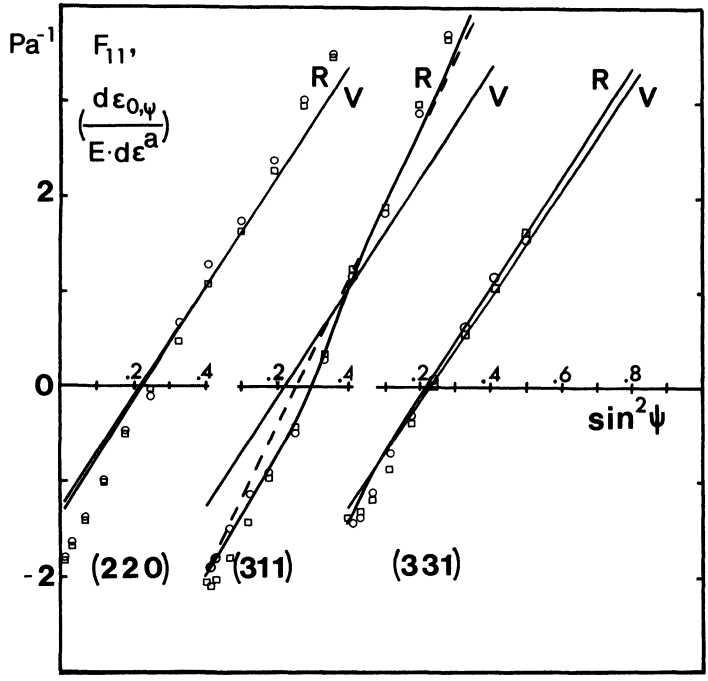

Figure 4 Same as Figure 3 for the lattice planes given in the figure. The distance for a given $\sin^2\psi$ between the circles ($\psi < 0°$) and the squares ($\psi > 0°$) gives an idea about the reproducibility of the ($d\varepsilon_{0,\psi}/E \cdot d\varepsilon^a$) values obtained from experiment.

fall outside the V–R range calculated for isotropic specimens. And that is what frequently happens with published $\frac{1}{2}S_2$ and S_1 data if they were obtained from an evaluation of experimental $\sin^2(\psi, \varepsilon^a)$ curves; examples for the case of Ni are given by Ruppersberg *et al.* (1980). Ignoring texture in the present case would yield $\frac{1}{2}S_2$ and S_1

Table 1 X-ray elastic constants calculated for random and textured specimen inserting for E and s_{ij} the values given in the text. (The Reuss curves of the textured specimen were observed to be close to linear!)

	(331)				(220)			
10^6 S_i	Random		Textured		Random		Textured	
mm^2/N	Voigt	Reuss	Voigt	Reuss	Voigt	Reuss	Voigt	Reuss
$-S_1$	1.20	1.14	1.26	1.38	1.20	1.30	1.26	1.54
$\frac{1}{2}S_2$	5.68	5.47	5.86	5.82	5.68	5.95	5.86	6.60

values which deviate by about 6 and 11% from the correct $\frac{1}{2}S_2$ and S_1 values, respectively; even though for the two reflections under consideration the $\mathbf{a}(\sin^2\psi)$ curves would be practically linear. It seems logical to assume that weak textures which are not immediately manifested in non linear $\mathbf{a}(\sin^2\psi)$ curves are frequently responsible for problems concerning the reproducibility of X-ray elastic constants.

We may summarize that the ODF formalism describes quite satisfactorily the variation of $\varepsilon_{\varphi,\psi}$ related to external stress and it seems logical to assume that the same is true of the effects of internal stress components. In a next stage we will no longer neglect the monoclinic distortions of the texture in order to obtain the ψ-splitting. And for further evaluation we will start with the most simple model for stress distribution, consisting in a two-axial surface stress having a gradient in the 3-direction. Stress components and gradients will be varied until most satisfactory fits are obtained for the general shape—omitting the small ripples—of all experimental $\mathbf{a}_{hkl}$ $(\sin^2\psi, \varphi)$ curves. Evaluation and proper consideration of possible texture gradients seem problematical, and their influence is probably small because the penetration depth corresponds to not much more than one or two grain diameters at maximum.

For finding the origin of the ripples we have to follow the $[(hkl), \psi, \varphi]$-hairlines (see Figure 1) for which they occur and search for regions in Λ where several affected hairlines intersect. It seems possible to find in this way the grain collectives which, during manufacture of the specimen, underwent special inhomogeneous plastic deformation.

Acknowledgements

We are indebted to HASYLAB for supporting this work and we thank the team of the Two-Axis Diffractometer for valuable help. The financial support from Deutsche Forschungsgemeinschaft is gratefully acknowledged. Simulation of the peak profile is supported by Siemens AG in the framework of III cooperation. We thank Dr. Burbach (Essen) and Dr. Esling (Metz) for many helpful discussions.

References

Barral M. and Sprauel J. M. (1983). in *Eigenspannungen*, eds. E. Macherauch and V. Hauk, DGM Oberursel, Vol. 2, p. 31.
Bollenrath, F., Hauk V. and Müller E. H. (1967). *Z. Metallkde.* **58,** 76.
Brakman C. M. (1983). *J. Appl. Cryst.* **16,** 325.

Bunge H. J. (1982). *Texture Analysis in Materials Science,* Butterworths, London.
Dölle H. and Hauk V. (1978). *Z. Metallkde.* **69,** 410.
Dölle H., Hauk V. and Zegers H. (1978). *Z. Metallkde.* **69,** 766.
Eckhardt M. and Ruppersberg H. (1987). In: Residual Stresses in Science and Technology, eds. E. Macherauch and V. Hauk, DGM Oberursel, Vol. 1, p. 377.
Hauk V., Nikolin H. J. and Weisshaupt H. (1980). *Z. Metallkde.* **76,** 226.
Ruppersberg H., Schmidt W. and Weiland H. (1980). *Z. Metallkde.* **71,** 475.
Ruppersberg H. (1981). *Proc. 2. europ. Tagung f. zerstörungsfreie Prüfung,* ed. Österr. Ges. f. zerstörungsfreie Prüfung, Wien, p.85.
Stickforth J. (1966) *Tech. Mitt. Krupp* **24,** 89.